

Probing non-standard $b\bar{b}h$ interaction at the LHC at $\sqrt{s} = 13$ TeV

Partha Konar,^a Biswarup Mukhopadhyaya,^b Rafiqul Rahaman,^c and Ritesh K. Singh^b

^a*Physical Research Laboratory, Ahmedabad - 380009, Gujarat, India*

^b*Department of Physical Sciences, Indian Institute of Science Education and Research Kolkata, Mohanpur, 741246, India*

^c*Regional Centre for Accelerator-based Particle Physics, Harish-Chandra Research Institute, HBNI, Chhatnag Road, Jhusi, Prayagraj 211019, India*

E-mail: konar@prl.res.in, biswarup@iiserkol.ac.in,
rafiqulrahaman@hri.res.in, ritesh.singh@iiserkol.ac.in

ABSTRACT: In the detailed probe of Higgs boson properties at the Large Hadron Collider, and in looking for new physics signatures in the electroweak symmetry breaking sector, the bottom quark Yukawa coupling has a crucial role. We investigate possible departure from the standard model value of $b\bar{b}h$ coupling, phenomenologically expressed in terms of a modification factor α_b , in $b\bar{b}$ -associated production of the 125-GeV scalar at the high-luminosity LHC. In a next-to-leading order estimate, we make use of a gradient boosting algorithm to improve in statistical significance upon a cut-based analysis. It is found possible to probe down to $\alpha_b = 3$ with more than 5σ significance, with $\mathcal{L} = 3000 \text{ fb}^{-1}$ and $\sqrt{s} = 13$ TeV, while the achievable limit at 95% C.L. is ± 1.95 .

KEYWORDS: Higgs coupling to b , Large Hadron Collider, gradient boosting

Contents

1	Introduction	1
2	The parametrisation of anomalous couplings	2
3	Cut-based analysis	5
4	Analysis based on the gradient boosting technique	6
5	Summary and conclusions	10
6	Acknowledgement	11
	References	11

1 Introduction

Whether the 125 GeV scalar discovered in 2012 [1, 2] is ‘the Higgs’ or ‘a Higgs’ is still an unresolved issue. Most importantly, its interaction strengths with relatively heavy fermions are not yet known precisely enough, in contrast to the interaction with gauge boson pairs, where the uncertainty is much lesser [3]. For example, the signal strength defined as $\mu_b = \frac{\sigma(b\bar{b})}{\sigma(b\bar{b})_{SM}}$, where the denominator corresponds to the rate predicted by the standard model (SM), lies in the range 0.84 – 1.24 [4]. Thus there is considerable scope of variation with respect to the standard model value. Here, we propose one way of reducing this uncertainty, by taking a fresh look at h -production associated with $b\bar{b}$ at the high-luminosity Large Hadron Collider (HL-LHC).

The $b\bar{b}$ -associated production of Higgs has been already studied [5–15], and the conclusion is that the rates are too small to make any difference, as far as the SM interaction is concerned. However, the rather large error-bar keeps alive the possibility of enhancement in the presence of new physics. This is reflected, for example, in two Higgs doublet models (2HDM) where regions in the parameter space with a large b -coupling of the 125 GeV scalar are still consistent with all experiments [16]. It is important, therefore, to look for clear signatures of such enhancement as the stamp of new physics.

Taking a model-independent standpoint, let us parametrize the modification factor for the $b\bar{b}h$ interaction strength by α_b , treated here as real, as

$$\alpha_b = \frac{y_b}{(y_b)_{SM}}. \quad (1.1)$$

Here $(y_b)_{\text{SM}} = \sqrt{2}m_b/v$ is the SM bottom Yukawa coupling ($v = 246$ GeV is the vacuum expectation value), and y_b is the bottom Yukawa coupling in a new physics model. The analysis of Higgs- p_T data with $\int \mathcal{L} dt = 35.9 fb^{-1}$ [17] already restricts α_b and α_c (its analogue for the charm) as $-1.1 \leq \alpha_b \leq +1.1$, $-4.9 \leq \alpha_c \leq +4.8$ at 95% C.L.. However, no other non-standard Higgs interaction is allowed in such an analysis, and thus the contributions to $h \rightarrow ZZ, \gamma\gamma$ bring in stringent constraints. However, in the absence of this restrictive assumption and allowance for ‘nuisance parameters’ relaxes the corresponding ranges to $[-8.5, 18.0]$ for α_b and $[-33.0, 38.0]$ for α_c . A more recent study [18] in the context of the high-luminosity LHC, running upto $3000 fb^{-1}$, yields the projected limits as $-2.0 \lesssim \alpha_b \leq +4.0$, $-10.0 \leq \alpha_c \leq +10.0$ at 95% C.L., once other non-standard interactions are not forbidden, and the branching ratios in the ZZ and $\gamma\gamma$ channels are not used as prior constraints.

We show here that α_b can be pinned down to an even shorter range by considering $pp \rightarrow b\bar{b}h$ in the high-luminosity run. In this channel, significant enhancement takes place at the production level itself for large α_b . This is of advantage, since the level of enhancement does not saturate with increasing α_b , unlike the effect on the branching ratio in the $b\bar{b}$ channel when the anomalous $b\bar{b}$ shows up in decays alone.

The resulting signal, where one looks for four b -jets with two of them close to the h -peak, is jacked up substantially for $\alpha_b \rightarrow 3.0$. However, it is also plagued by backgrounds, including four b -jets from QCD, $b\bar{b}Z$ production, and also QCD production of $2b2c$, with two c -quark jets faking b 's.

The backgrounds pose larger next-to-leading order (NLO) QCD corrections strengths than that of the signal, thus making the signal significance smaller at NLO than the leading-order (LO) values. Our analysis reveals how the resulting loss in signal significance due to the NLO QCD effects can be ameliorated by adopting an algorithm based on Boosted Decision Trees (BDT)—in particular, the gradient boosting technique.

In section 2, we provide an outline of the framework to operate within, with α_b (and α_c) taken as purely phenomenological parameters, with no bar *prima facie* on other non-standard interactions. We also discuss the signal and all major irreducible background processes involved in the present analysis. Sections 3 and 4 contains, respectively, report on cut-based and BDT-based machine learning analyses. We summarise and conclude in section 5.

2 The parametrisation of anomalous couplings

We are interested in the $b\bar{b}$ -associated Higgs production followed by the Higgs decaying to a pair of b at the LHC, thus resulting in a $4b$ final state. The representative Feynman diagrams for the $b\bar{b}h$ production at the LHC are shown in Figure 1. The $h \rightarrow b\bar{b}$ decay is not shown in the diagrams. The α_b also appears in the decay vertex of the $h \rightarrow b\bar{b}$ apart from the production process. The total cross section of the signal

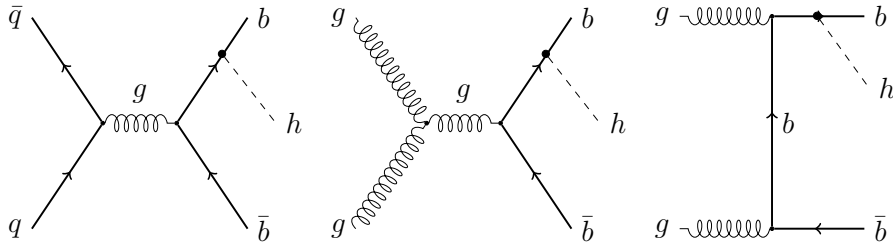


Figure 1. Representative Feynman diagram for the $b\bar{b}h$ production at the LHC at leading order (LO). The non-standard $b\bar{b}h$ coupling is shown by the blobs. Higgs decays further through $h \rightarrow b\bar{b}$. The second blob in such vertex are not shown in the diagrams.

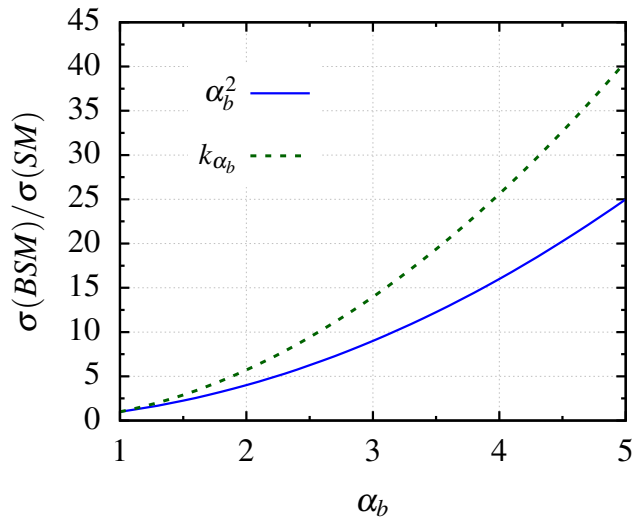


Figure 2. The enhancement factor received in the signal cross section over SM, as defined at Eq. 2.2 is shown for variation of modification factor in $b\bar{b}h$ interaction strength α_b .

with α_b will be,

$$\sigma_{b\bar{b}h \rightarrow 4b}(\alpha_b) = \alpha_b^2 \sigma_{b\bar{b}h}(SM) \times \frac{\alpha_b^2 \Gamma(h \rightarrow b\bar{b})}{\Gamma_h(\alpha_b)} \quad (2.1)$$

enhancing the SM cross section by a factor of

$$k_{\alpha_b} = \frac{\sigma_{b\bar{b}h \rightarrow 4b}(\alpha_b)}{\sigma_{b\bar{b}h \rightarrow 4b}(SM)} = \alpha_b^2 \frac{\alpha_b^2 \Gamma_h(SM)}{\Gamma_h(\alpha_b)}. \quad (2.2)$$

The enhancement factor for the signal cross section over the SM is shown in Figure 2 with varying α_b for $B(h \rightarrow b\bar{b}) \approx 60\%$ [19]. The solid/blue line represents the factor when the new physics effect is accounted for only in the production part; the dashed/green line, however, represents the enhancement factor when the new physics is accounted for in both production as well as in the decay process.

The major backgrounds to the $4b$ final state comes from QCD $4b$ -jets, QCD $2b2c$ with the c -quarks faking as b -jets, $b\bar{b}Z$ production, and hZ production. We

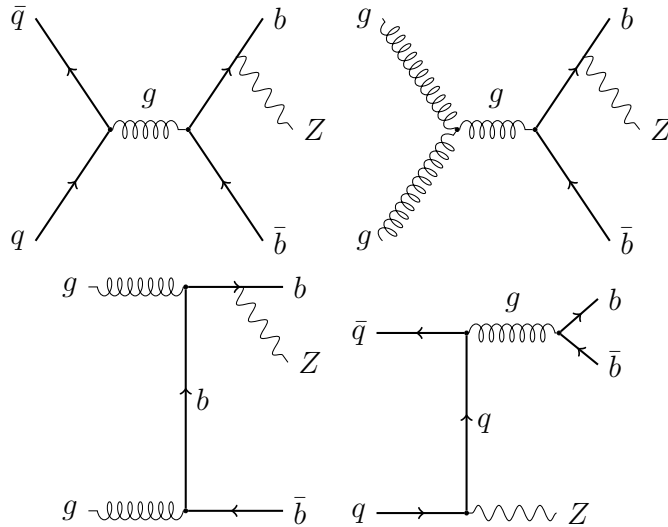


Figure 3. Representative Feynman diagram for the topologically very similar background process through $b\bar{b}Z$ production at the LHC at LO.

Process	LO cross section(pb)
$bbh \rightarrow 4b$ ($\alpha_b = 1$)	$5.386^{+29.5\%}_{-21.6\%}(\text{scale}) \pm 12.4\%(PDF) \times 10^{-3}$
$bbZ \rightarrow 4b$	$2.082^{+26.9\%}_{-20.1\%}(\text{scale}) \pm 11.5\%(PDF)$
QCD- $4b$	$118.194^{+60.9\%}_{-35.5\%}(\text{scale}) \pm 12.4\%(PDF)$
QCD- $2b2c$	$636.098^{+60.6\%}_{-35.4\%}(\text{scale}) \pm 12.6\%(PDF)$
$hZ \rightarrow 4b$	$0.01764^{+4.7\%}_{-5.8\%}(\text{scale}) \pm 6.1\%(PDF)$

Table 1. Parton level cross sections of signal and the major background processes at the leading order (LO), after applying the generator level event selection cuts of $p_T(b) > 30$ GeV, $\Delta R(b, b) > 0.4$, $\eta_b < 2.5$ using the scale choice of $\mu_R = \mu_F = \mu_0 = (2m_b + m_h)/2$.

ignore the QCD $4j$ process as the probability of four light jets faking as four b -jets is insignificantly small. The background $b\bar{b}Z$, Feynman diagrams shown in Figure 3, has the same topology as the signal $b\bar{b}h$, and thus expected to be irreducible from the signal. The QCD and the hZ backgrounds, however, are expected to be reducible for having a different topology than that of the signal. The leading order cross sections for the signal and the backgrounds for the $4b$ final state estimated in the MADGRAPH5_aMC@NLO v2.6.4 (mg5_aMC) [20] package with a generator level cuts of $p_T(b) > 30$ GeV, $\Delta R(b, b) > 0.4$, and $\eta_b < 2.5$ are presented in the Table 1. We use a fixed renormalization (μ_R) and factorization (μ_F) scale of $\mu_R = \mu_F = \mu_0 = (2m_b + m_h)/2$ for the signal as well as for the backgrounds motivated by the $b\bar{b}h$ production topology. The scale uncertainties, shown in Table 1, are estimated by

Signal & background process		No. of events @ LO		No. of events @ NLO	
		cut1	cut2	cut1	cut2
S :	$bbh \rightarrow 4b$	33511	30867	38895	34946.8
B_1 :	$bbZ \rightarrow 4b$	846715	682871	1.67229×10^6	1.33163×10^6
B_2 :	QCD - $4b$	4.24088×10^7	3.36035×10^7	6.81198×10^7	5.07642×10^7
B_3 :	QCD- $2b2c$	1.53389×10^7	1.1986×10^7	2.15198×10^7	1.68568×10^7
B_4 :	$hZ \rightarrow 4b$	7817	7168	20177	18244
Significance ($\frac{S}{\sqrt{B}}$)		4.38	4.54	4.07	4.21

Table 2. Expected number of events for the signal as well as the backgrounds and signal significance (S/\sqrt{B}) at $\mathcal{L} = 3000 \text{ fb}^{-1}$ with $\alpha_b = 3$ at LO as well as at NLO for $\mu_R = \mu_F = \mu_0 = (2m_b + m_h)/2$ for two cuts region given in Eq. 3.1.

varying the μ_R and μ_F in the range of $0.5\mu_0 \leq \mu_R, \mu_F \leq 2\mu_0$, with the constraint $0.5 \leq \mu_R/\mu_F \leq 2$. We use the NNPDF3.0 [21] sets of parton distribution functions (PDFs) with $\alpha_s(m_Z) = 0.118$ for our calculations. A branching ratio of 60% is used for the $h \rightarrow b\bar{b}$ decay [19] with $m_h = 125 \text{ GeV}$.

3 Cut-based analysis

We generated events for the signal and the backgrounds in mg5_aMC at LO and NLO with chosen renormalization and factorization scale. The QCD- $2b2c$ background, however, is generated only at LO, and it is used for NLO analysis with a k -factor of 1.4 taken from the QCD- $4b$ background. The showering and hadronization of the events are performed by PYTHIA8 [22] followed by the detector simulations by Delphes-3.4.2 [23]. We estimated the expected number of events with four b -tagged jets for the signal with $\alpha_b = 3$ and the backgrounds after detector simulations at an integrated luminosity of $\mathcal{L} = 3000 \text{ fb}^{-1}$ for the following two kinematical regions:

$$\text{Event selection (cut1)} : p_T(b) > 20 \text{ GeV}, \Delta R(b, b) > 0.5, \eta_b < 2.5, \quad (3.1)$$

$$\text{Event selection (cut2)} : \text{cut1} + \text{at least one } m_{bb} \in [100, 150] \text{ GeV} \quad (3.2)$$

and present them in Table 2 for $\mu_R = \mu_F = \mu_0 = (2m_b + m_h)/2$. For the cut2, we select events with at least one b pair with invariant mass in the range $[100, 150]$, thus emulating a Higgs candidate. We calculate the signal significance, defined by S/\sqrt{B} with S being signal events and B being total background events, for the two cut region, and they are shown in the lowest row of Table 2. A $b\bar{b}h$ signal with $\alpha_b = 3$

can be observed with a significance of 4.54 (4.21) at LO (NLO) in the `cut2` region at an integrated luminosity of $\mathcal{L} = 3000 \text{ fb}^{-1}$ for renormalization and factorization scale of $\mu_R = \mu_F = \mu_0 = (2m_b + m_h)/2$. The signal significance for other renormalization and factorization scales namely $\mu_R = \mu_F = \mu_0/2$, $2\mu_0$ are also shown in the next section for comparison. The QCD corrections for the signal being much smaller compared to the same for the QCD backgrounds, and the shape of the distributions of the variables being similar for LO and NLO, the signal significance is smaller at NLO compared to the LO result. Other than the `cut2` regions, cuts such as p_T , H_T , m_{4b} , \cancel{E}_T on the b -jets do not improve the signal significance. These variables, however, in certain combinations, may improve the signal significance, which we explore with the gradient boosting technique in the next section.

4 Analysis based on the gradient boosting technique

After estimating a maximally achievable signal significance with a simple cut-based analysis (`cut2` in Eq. (3.1)), we further explore the possibility of improving the significance by a Machine Learning technique namely *Gradient Boosted Decision Trees* (gradient BDT) [24] by employing various kinematical variables. We use the package `XGBoost` [24] as a toolkit for the gradient boosting. We construct these following kinematical features as input for the gradient boosting:

- Transverse momentum of each of the four leading b -tagged jets $p_T(b_i)$ (4 variables),
- Total invariant mass of all four leading b -tagged jets m_{4b} and inclusive variables, such as, missing transverse momentum MET , global mass scale variable H_T (3 variables),
- Set of all b -jet pair invariant masses $m_{b_i b_j}$, and b -pair transverse momentum $p_T(b_i b_j)$ from all four leading b -tagged jets (12 variables),
- θ -angle (measured w.r.t. the boost of $4b$ -system) and pseudo-rapidity of each b -tagged jet $\cos\theta(b_i)$, η_{b_i} (8 variables),
- Angular and azimuthal angle separation between set of all b -jet pairs $\Delta R(b_i b_j)$, $\Delta\phi(b_i b_j)$ (12 variables),
- Angular and azimuthal angle separation between the ‘invariant-mass based reconstructed’ Higgs candidate (composed of two b -tagged jets - so called b_1 and b_2) from other two b -tagged jet candidates $\Delta R(hb_3)$, $\Delta R(hb_4)$, $\Delta\phi(hb_3)$, $\Delta\phi(hb_4)$ (4 variables),
- Angular and azimuthal angle separation between the ‘angular-separation based reconstructed’ Higgs candidate (composed of two b -tagged jets - so called b_1

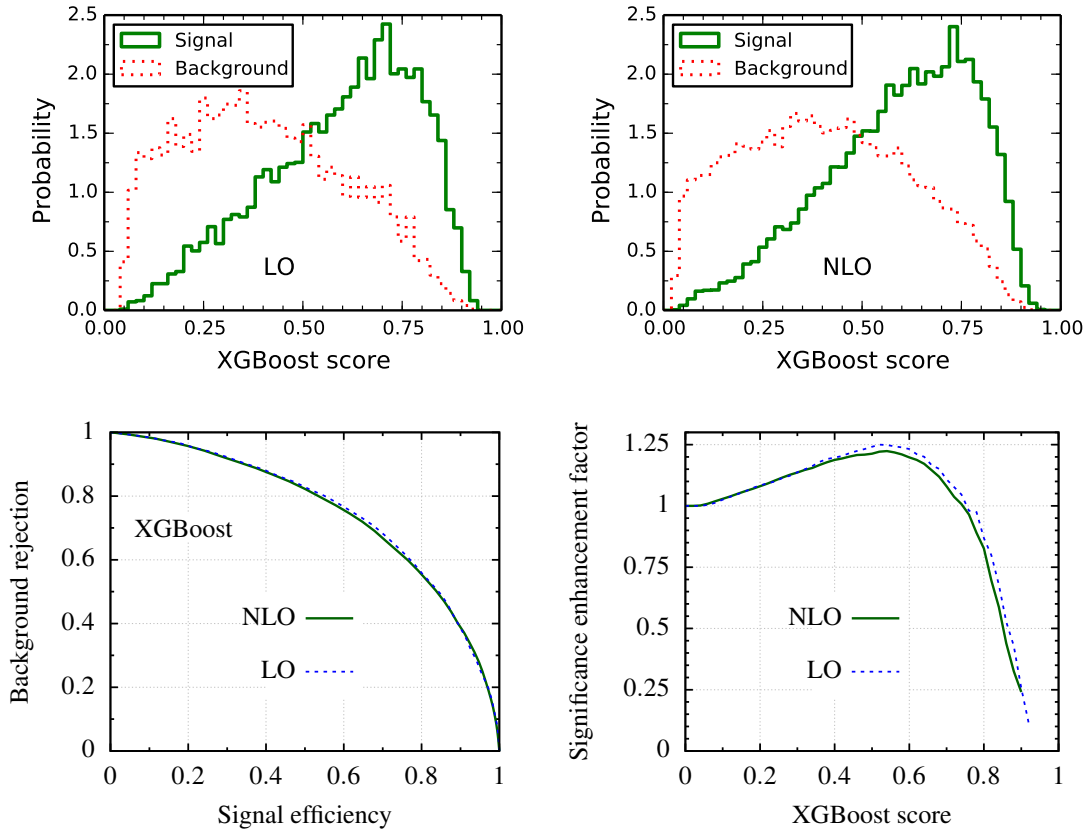


Figure 4. Normalised distribution of BDT response for the signal and background processes representing relative separability based on the XGBoost score cut for LO (*top-left*) and NLO (*top-right*). Corresponding performance in terms of ROC (receiver operating characteristic) curve shown in *bottom-left* curve. Also the *right-bottom* plot is for significance enhancement factor depending on the XGBoost score cut for $\mu_R = \mu_F = \mu_0 = (2m_b + m_h)/2$.

and b_2) from other two b -tagged jet candidates $\Delta R(h'b'_3)$, $\Delta R(h'b'_4)$, $\Delta R(b'_3b'_4)$, $\Delta\phi(h'b'_3)$, $\Delta\phi(h'b'_4)$, $\Delta\phi(b'_3b'_4)$ (6 variables).

The number in parentheses at the end of each item represents the total number of features in each item, giving a total of 49 features. The features are reconstructed as follows: The Higgs candidate (h) is reconstructed with the b -pair close to 125 GeV invariant mass. These two b 's are labelled as b_1 and b_2 ordered by their p_T . The other two b 's are labelled as b_3 and b_4 , also ordered by their p_T . On the other hand, the primed Higgs candidate (h') is reconstructed using the lowest ΔR of the b -pairs. The b'_i are labelled in a similar way as done in the un-primed case.

We use an equal number of events for the signal and background events to classify them using the *train* module of XGBoost. The backgrounds are mixed with the ratio of their corresponding rates in *cut2* region given in Table 2. We use 80% of the total dataset for training purposes and the rest 20% for testing purposes. At first,

		@LO	@NLO		
Scale choice ($\mu_R = \mu_F = \mu_0$)		μ_0	$\mu_0/2$	μ_0	$2\mu_0$
Cut-based significance ($\frac{S}{\sqrt{B}}$)		4.54	2.92	4.21.	5.06
XGBoost	Signal efficiency (ϵ_S)	67.7%	74.3%	70.8%	67.3%
	Background rejection ($\bar{\epsilon}_B$)	70.7%	63.1%	65.9%	68.5%
	Enhancement factor ($\frac{\epsilon_S}{\sqrt{1-\bar{\epsilon}_B}}$)	1.25	1.22	1.2	1.2
	Maximum significance ($\frac{S}{\sqrt{B}} \times \frac{\epsilon_S}{\sqrt{1-\bar{\epsilon}_B}}$)	5.67	3.56	5.05	6.07

Table 3. Comparison of signal efficiency ϵ_S , background rejection $\bar{\epsilon}_B \equiv (1-\epsilon_B)$, efficiency factor and significance between the leading order (LO) calculation and the next to leading order (NLO). Both cut and count based and XGBoost analysis results are shown at the luminosity $\mathcal{L} = 3000 \text{ fb}^{-1}$ after the final event selection as in `cut2`, for a moderate value of modification factor, $\alpha_b = 3$. Also the effect of variation in renormalization and factorization scale choice at the NLO pointed out in additional columns. Note for the XGBoost analysis, results are shown for a choice of XGBoost score cut where the maximum significance is achievable.

we vary the XGBoost parameters to obtain a combination of them for a maximum accuracy to classify the signal and the backgrounds. We obtain a maximum accuracy of $69.13\% \pm 0.44\%$ (1σ) for LO events and $68.06\% \pm 0.23\%$ (1σ) for NLO events at $\mu_R = \mu_F = \mu_0$ for the following combination of the parameters' values [25]:

- Step size shrinkage: $\eta = 0.1$,
- Maximum depth of a tree: $max_depth = 50$,
- Subsample ratio of the training instances: $subsample = 0.9$,
- subsample ratio of columns when constructing each tree: $colsample_bytree = 0.3$,
- Minimum loss reduction required to make a further partition on a leaf node of the tree: $\gamma = 1.0$,
- L2 regularization term on weights: $\lambda = 50.0$,
- L1 regularization term on weights: $\alpha = 1.0$,
- Number of parallel trees constructed during each iteration: $num_parallel_tree = 8$.

The final probability distributions of the output of the BDT network (XGBoost score) for the signal and the total backgrounds are shown in Figure 4 in the *top-row* to

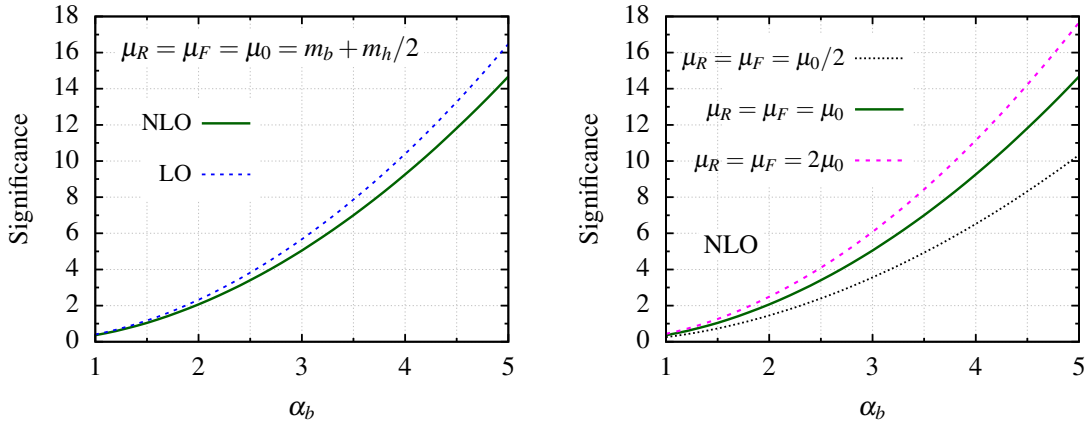


Figure 5. Achievable total significance as a function of modification factor for the $hb\bar{b}$ interaction strength α_b at LO and NLO in *left-panel* with renormalization and factorization scales at $\mu_0 = m_b + m_h/2$ for $\mathcal{L} = 3000 \text{ fb}^{-1}$. The *right-panel* shows the scale variance of such significance at NLO considering two extreme cases of changing both the scales with a factor of half and a factor of two.

show their separability for LO (*left*) as well as for NLO (*right*). The signal efficiency versus the background rejection curves for LO and NLO are shown in Figure 4 in the *left-bottom-panel*. The larger the area under the curves of signal efficiency versus the background rejection, the better is the separability between the signal and the background. Compared to the LO, the NLO events are less distinguishable, thus reduces the background rejection. The XGBoost score cut is varied to obtain the signal efficiency ϵ_S , background rejection $\bar{\epsilon}_B \equiv (1 - \epsilon_B)$ for the maximum factor by which the significance can be improved. The significance enhancement factor ($\frac{\epsilon_S}{\sqrt{1-\epsilon_B}}$) w.r.t. the XGBoost score cut is shown in the *right-bottom-panel* in Figure 4. For a XGBoost score of 0.52 (0.50), 67.7% (70.8%) signal remains rejecting a total of 70.7% (65.9%) background for LO (NLO) events, thus maximally enhancing the signal significance by a factor of 1.25 (1.2). Thus the total significance after the BDT analysis becomes $4.54 \times 1.25 = 5.67$ ($4.21 \times 1.2 = 5.058$) at LO (NLO). The combined result of cut-based and XGBoost at NLO are shown in Table 3 in the second and fourth column for LO and NLO, respectively. Table 3 also contains result for renormalization and factorization scale choice $\mu_0/2$ and $2\mu_0$ for NLO; The reason being discussed below.

The QCD correction strengths and the shape of the distributions for the kinematical variable change as the renormalization and factorization scale are changed for the signal as well as for backgrounds. As a result, our results in cut-based as well as in BDT-based analysis are expected to be different for different μ_R and μ_F . So, we repeat all analyses for two extreme cases of μ_R and μ_F with a factor of half and one, i.e., $\mu_R = \mu_F = \mu_0/2$, μ_0 , $2\mu_0$ apart from μ_0 and obtain the results. The results are shown in Table 3 for $\mu_R = \mu_F = \mu_0/2$, μ_0 , $2\mu_0$. The results for μ_0 are

repeated for comparison. The QCD correction strength increase for the signal as the scale choices are doubled to $2\mu_0$, while it decreases as the scale choices are reduced to $\mu_0/2$. However, the QCD corrections remain roughly the same for the backgrounds, specially for the dominant $4b$ QCD background. As a result, as the scale choices are doubled, the signal significance improves by 25%, but it decreases when the scale choices are halved at the cut-based analysis. In the XGBoost result, the significance enhancement factor, however, increase a little due to the increase in signal efficiency for lower-scale choices.

Till now we have shown the results for $\alpha_b = 3$, i.e., for a fixed value of the new physics parameter. The total signal significance, including cut-based and XGBoost, are computed for varying α_b , and they are shown in Figure 5 for $\mu_R = \mu_F = \mu_0$ at LO and NLO in *left-panel* at $\mathcal{L} = 3000 \text{ fb}^{-1}$. The *right-panel* in Figure 5 shows the comparison of signal significance for three different scale choices namely $\mu_0/2$, μ_0 , and $2\mu_0$ at NLO for the same luminosity $\mathcal{L} = 3000 \text{ fb}^{-1}$. The limits on α_b is obtained to be ± 1.95 at 95% C.L. at NLO for $\mu_R = \mu_F = \mu_0$, see Figure 5 *left-panel*. The limits on α_b is tighter for higher scale choices and weaker for lower scale choices, as can be seen in the *right-panel*.

It appears that the strengths of QCD corrections for the backgrounds are always higher than that for the signal for a range of renormalization and factorization scales, thus making the signal significance smaller for NLO than LO for both cut-based and XGBoost analysis. A 5σ discovery significance is achievable for a moderate value of $\alpha_b = 3$ at a projected luminosity of 3000 fb^{-1} at the LHC.

5 Summary and conclusions

While LHC is emphatically looking for any indication of elusive new physics, hints of that can already be hidden in our Higgs data. Precision measurements of Higgs coupling with third-generation quarks are thus crucial in indirect probes on the physics beyond the standard model. In this present work, we probe the non-standard $hb\bar{b}$ coupling parametrized in a model-independent standpoint in $b\bar{b}$ -associated production of Higgs. We point out the importance and effectiveness of this channel in uncovering the modification factor in $hb\bar{b}$ interaction strength.

With a detailed detector level simulation, we devised a phase space region to emulate a Higgs peak in the signal and also to regulate the background processes. We obtain a moderate signal significance showing the outcome both at LO as well as at NLO for a choice of modification factor $\alpha_b = 3$ at high luminosity LHC. This cut-based significance is further refined upon by gradient boosted techniques later on. Overall, the NLO result is slightly weaker than that of LO. We also investigate the effect of (renormalization and factorization) scale variation on the results at NLO and observe a significant variation, with better results at relatively higher scale values.

The limit on α_b , which is ± 1.95 at 95% C.L. for $\mathcal{L} = 3000 \text{ fb}^{-1}$, is surpassing the existing results in literature.

During the concluding stage of study, we came across reference [26], where an anomalous $hb\bar{b}$ interaction has been investigated via the Higgs decay channel $h \rightarrow \gamma\gamma$, in the context of higher energies and luminosities than those envisioned currently for the HL-LHC. Our study differs from theirs in several ways. First, by concentrating on the $b\bar{b}$ decay mode, one expects considerably larger event rates. Secondly, it also entails more severe backgrounds. Thirdly, next-to-leading order QCD effects are more non-trivial, not only for the backgrounds but for the signal as well. We have shown how to overcome the second and third issues, especially with the help of gradient boosting techniques, and thus improve upon hitherto estimated levels of constraining α_b at the HL-LHC, with $\int \mathcal{L} dt = 3000 \text{ fb}^{-1}$.

6 Acknowledgement

The work of PK is supported by Physical Research Laboratory (PRL), Department of Space, Government of India. The work of RR is partially supported by funding available from the Department of Atomic Energy, Government of India, for the Regional Centre for Accelerator-based Particle Physics (RECAPP), Harish-Chandra Research Institute. The work of RKS is partially supported by SERB, DST, Government of India through the project EMR/2017/002778.

References

- [1] CMS Collaboration, S. Chatrchyan *et al.*, *Observation of a new boson at a mass of 125 GeV with the CMS experiment at the LHC*, *Phys. Lett.* **B716** (2012) 30–61, [arXiv:1207.7235 \[hep-ex\]](#).
- [2] ATLAS Collaboration, G. Aad *et al.*, *Observation of a new particle in the search for the Standard Model Higgs boson with the ATLAS detector at the LHC*, *Phys. Lett.* **B716** (2012) 1–29, [arXiv:1207.7214 \[hep-ex\]](#).
- [3] ATLAS Collaboration, G. Aad *et al.*, *Combined measurements of Higgs boson production and decay using up to 80 fb⁻¹ of proton-proton collision data at $\sqrt{s} = 13$ TeV collected with the ATLAS experiment*, *Phys. Rev. D* **101** no. 1, (2020) 012002, [arXiv:1909.02845 \[hep-ex\]](#).
- [4] CMS Collaboration, A. M. Sirunyan *et al.*, *Observation of Higgs boson decay to bottom quarks*, *Phys. Rev. Lett.* **121** no. 12, (2018) 121801, [arXiv:1808.08242 \[hep-ex\]](#).
- [5] C. Balazs, J. L. Diaz-Cruz, H. J. He, T. M. P. Tait, and C. P. Yuan, *Probing Higgs bosons with large bottom Yukawa coupling at hadron colliders*, *Phys. Rev.* **D59** (1999) 055016, [arXiv:hep-ph/9807349 \[hep-ph\]](#).

- [6] R. V. Harlander and W. B. Kilgore, *Higgs boson production in bottom quark fusion at next-to-next-to leading order*, *Phys. Rev. D* **68** (2003) 013001, [arXiv:hep-ph/0304035](#).
- [7] S. Dittmaier, M. Krämer, and M. Spira, *Higgs radiation off bottom quarks at the Tevatron and the CERN LHC*, *Phys. Rev.* **D70** (2004) 074010, [arXiv:hep-ph/0309204](#) [[hep-ph](#)].
- [8] S. Dawson, C. Jackson, L. Reina, and D. Wackerath, *Exclusive Higgs boson production with bottom quarks at hadron colliders*, *Phys. Rev. D* **69** (2004) 074027, [arXiv:hep-ph/0311067](#).
- [9] J. M. Campbell, S. Dawson, S. Dittmaier, C. Jackson, M. Kramer, F. Maltoni, L. Reina, M. Spira, D. Wackerath, and S. Willenbrock, *Higgs boson production in association with bottom quarks*, in *Physics at TeV colliders. Proceedings, Workshop, Les Houches, France, May 26-June 3, 2003*. 2004. [arXiv:hep-ph/0405302](#) [[hep-ph](#)].
- [10] S. Dawson, C. Jackson, L. Reina, and D. Wackerath, *Higgs production in association with bottom quarks at hadron colliders*, *Mod. Phys. Lett. A* **21** (2006) 89–110, [arXiv:hep-ph/0508293](#).
- [11] M. Wiesemann, R. Frederix, S. Frixione, V. Hirschi, F. Maltoni, and P. Torrielli, *Higgs production in association with bottom quarks*, *JHEP* **02** (2015) 132, [arXiv:1409.5301](#) [[hep-ph](#)].
- [12] S. Forte, D. Napoletano, and M. Ubiali, *Higgs production in bottom-quark fusion in a matched scheme*, *Phys. Lett. B* **751** (2015) 331–337, [arXiv:1508.01529](#) [[hep-ph](#)].
- [13] B. Jäger, L. Reina, and D. Wackerath, *Higgs boson production in association with b jets in the POWHEG BOX*, *Phys. Rev. D* **93** no. 1, (2016) 014030, [arXiv:1509.05843](#) [[hep-ph](#)].
- [14] M. Bonvini, A. S. Papanastasiou, and F. J. Tackmann, *Matched predictions for the $b\bar{b}H$ cross section at the 13 TeV LHC*, *JHEP* **10** (2016) 053, [arXiv:1605.01733](#) [[hep-ph](#)].
- [15] N. Deutschmann, F. Maltoni, M. Wiesemann, and M. Zaro, *Top-Yukawa contributions to bbH production at the LHC*, *JHEP* **07** (2019) 054, [arXiv:1808.01660](#) [[hep-ph](#)].
- [16] D. Fontes, J. C. Romão, R. Santos, and J. a. P. Silva, *Large pseudoscalar Yukawa couplings in the complex 2HDM*, *JHEP* **06** (2015) 060, [arXiv:1502.01720](#) [[hep-ph](#)].
- [17] CMS Collaboration, A. M. Sirunyan *et al.*, *Measurement and interpretation of differential cross sections for Higgs boson production at $\sqrt{s} = 13$ TeV*, *Phys. Lett.* **B792** (2019) 369–396, [arXiv:1812.06504](#) [[hep-ex](#)].
- [18] M. Cepeda *et al.*, *Report from Working Group 2, CERN Yellow Rep. Monogr.* **7** (2019) 221–584, [arXiv:1902.00134](#) [[hep-ph](#)].

- [19] **Particle Data Group** Collaboration, M. Tanabashi *et al.*, *Review of Particle Physics*, *Phys. Rev. D* **98** no. 3, (2018) 030001.
- [20] J. Alwall, R. Frederix, S. Frixione, V. Hirschi, F. Maltoni, O. Mattelaer, H. S. Shao, T. Stelzer, P. Torrielli, and M. Zaro, *The automated computation of tree-level and next-to-leading order differential cross sections, and their matching to parton shower simulations*, *JHEP* **07** (2014) 079, [arXiv:1405.0301 \[hep-ph\]](#).
- [21] **NNPDF** Collaboration, R. D. Ball *et al.*, *Parton distributions for the LHC Run II*, *JHEP* **04** (2015) 040, [arXiv:1410.8849 \[hep-ph\]](#).
- [22] T. Sjöstrand, S. Ask, J. R. Christiansen, R. Corke, N. Desai, P. Ilten, S. Mrenna, S. Prestel, C. O. Rasmussen, and P. Z. Skands, *An introduction to PYTHIA 8.2*, *Comput. Phys. Commun.* **191** (2015) 159–177, [arXiv:1410.3012 \[hep-ph\]](#).
- [23] **DELPHES 3** Collaboration, J. de Favereau, C. Delaere, P. Demin, A. Giammanco, V. Lemaître, A. Mertens, and M. Selvaggi, *DELPHES 3, A modular framework for fast simulation of a generic collider experiment*, *JHEP* **02** (2014) 057, [arXiv:1307.6346 \[hep-ex\]](#).
- [24] T. Chen and C. Guestrin, *XGBoost: A Scalable Tree Boosting System*, [arXiv:1603.02754 \[cs.LG\]](#).
- [25] *XGBoost Parameters*.
<https://xgboost.readthedocs.io/en/latest/parameter.html>.
- [26] C. Grojean, A. Paul, and Z. Qian, *Resurrecting $b\bar{b}h$ with kinematic shapes*, [arXiv:2011.13945 \[hep-ph\]](#).